Spring 2012

# A three-dimensional transient simulation of an electrochemical magnetohydrodynamics cell with micro and millielectrode: A unified reconciliation of theory and experiment

Cajon Gonzales



Department:

# A THREE-DIMENSIONAL TRANSIENT SIMULATION OF AN ELECTROCHEMICAL MAGNETOHYDRODYNAMICS CELL WITH MICRO AND MILLIELECTRODE: A UNIFIED RECONCILIATION OF THEORY AND EXPERIMENT

by

CAJON GONZALES

A THESIS

Presented to the Faculty of the Graduate School of the

MISSOURI UNIVERSITY OF SCIENCE AND TECHNOLOGY

In Partial Fulfillment of the Requirements for the Degree

MASTER OF SCIENCE IN MECHANICAL ENGINEERING

2012

Approved by

Kakkattukuzhy M. Isaac, Advisor
Nicholas Leventis
Keith J. Nisbett

# PUBLICATION THESIS OPTION

This thesis has been prepared in the style utilized by the Journal of American Chemical Society. Pages 1-28 will be submitted for publication in that journal.

# ABSTRACT

Even though electrochemically induced magnetohydrodynamic (MHD) convection is a straightforward inexpensive method for moving fluids in confined spaces as for example during electrodeposition, stripping voltammetry, or in microfluidics, efficient quantitative models only recently have begun to appear. This is traced to complex mathematics that have prevented development of analytical expressions, e.g., for mass-transfer limited currents in analogy to the well-known Levich equation for the rotating electrode. Thus, related literature expressions remain mainly phenomenological concerning particular cell geometries or applications. Here, using such reports as points of departure, we validate a computationally rigorous description of the magnetoelectrochemical problem and define the relative significance of all system parameters. For this we use a three-dimension transient numerical simulation and establish that the full problem is adequately described by the conservation of momentum (modified Navier-Stokes equation), conservation of mass, and conservation of species (Fick's second law augmented with convection). These three equations are coupled by the Faradaic current given as a function of the flux of the redox active species to the working electrode. Computations are performed in the regime of milli and microelectrodes ranging from 250 μm in diameter to 16 mm, both with and without a magnetic field. Millielectrodes without a magnetic field generate diffusion-controlled voltammograms, and with the magnetic field vector parallel to the electrode surface, generate sigmoidal-shaped steady-state voltammograms. The Lorentz force was applied to the whole solution, but migrational current was ignored, so only in the presence of a concentration gradient was the Lorentz force applied. This region is in the near field of the working electrode and renders the placement of the counter electrode unimportant. The limiting current generated captures most of the experimental observations.

# ACKNOWLEDGEMENTS

Knowledge does not come with an easy course; I have had the great opportunity to take that course with amazing love and support from all sources. I would like to offer my sincerest gratitude to Kakkattukuzhy M. Isaac, my advisor and mentor. When I became his student I came with only curiosity and meager mathematical skills, and he molded the way that I do research. He has done much more than that though, touching my life in unknown ways.

Another individual Nicholas Leventis poured his knowledge of electrochemistry into me and spent a great amount of time mentoring me and for that I am forever grateful. Dr. Leventis provided a spark of enthusiasm in a time of need for me which helped me overcome great obstacles in my research. Dr. Nisbett offered confidence and ignited the need to solidify why I was doing this research which helped me stay on task and see this through to the end.

I would like to thank the National Science Foundation for providing financial support and the Mechanical Engineering Department for allowing me to teach to students. Also I would like to thank everyone in IT that helped me through the issues with FLUENT® and the NIC.

Others that helped me through this include: Jason Iverson, Caleb Baumgart, everyone in the Hydro and Turbulent mixing lab, Debamoy Sen, Naveen Chandrasekaran, Dr. Ingrid Fritsch and her research team, and anyone who listened to me ramble on about subjects that didn't make any sense to them.

Lastly, I wanted to thank my fiancée Anna Lepley who is stronger than anyone that I have ever met in my life. My family for their undying support in whatever I choose to do.

# TABLE OF CONTENTS

# LIST OF ILLUSTRATIONS

Page

## Introduction

The earliest work on electrolysis in the magnetic field is credited to Michael Faraday.[1] The prevalent macroscopic phenomenon is convection (stirring) owing to Lorentz forces on moving charges and paramagnetic forces on magnetic dipoles in field gradients moving towards regions of higher field intensity. In solution, moving charges or dipoles collide with the solvent molecules and transfer momentum. Per unit volume element of the liquid that contains moving charges or paramagnetic species the Lorentz body force density, $\vec{F}_B$, is given by eq 1, and the field-gradient paramagnetic force, $\vec{F}_{\nabla B}$, by eq 2. Where, $\vec{j}$ is the ionic current density, $\vec{j} = \vec{i} / A$, with $\vec{i}$ being the total current

$$\vec{F}_B = \vec{j} \times \vec{B} \tag{1}$$

$$\vec{F}_{\nabla B} = 2N_A C_m \frac{(g\mu_B)^2}{4kT} \left(\vec{B} \cdot \nabla\right) \vec{B} \tag{2}$$

flowing through the ionic conductor, and $A$ the cross-sectional surface area of the electrolytic conductor at the point where the volume element is considered), $\vec{B}$ is the magnetic field strength, $N_A$ is Avogadro's number, $g$ the spectroscopic splitting factor, $\mu_B$ the Bohr magneton, $k$ the Boltzmann constant, $T$ the absolute temperature, and $C_m$ the concentration of species $m$, which in the spirit of eq 2 is paramagnetic. It is noted further that there is also a third, rather controversial, paramagnetic body force, $\vec{F}_{\nabla C}$, that does not arise as the sum of forces on individual ions or magnetic dipoles, but is applied directly on volume elements that contain concentration gradients of paramagnetic species.[2,3] $\vec{F}_{\nabla C}$ is given by eq 3 and does not depend on field gradients.[4-7]

$$\vec{F}_{\nabla C} = N_A \frac{(g\mu_B)^2}{4kT} \vec{B}^2 \left(\nabla C_m\right) \tag{3}$$

Conservation of charge dictates that the electronic current flowing outside an electrochemical cell is equal to the ionic current, $\vec{i}$, flowing inside. Electron transfer occurs at the electrode solution interface which is carried out utilizing a redox species, which generates paramagnetic species (e.g., radicals) in the vicinity of the electrode, that give rise to $\vec{F}_{\nabla B}$ and $\vec{F}_{\nabla C}$.

From a practical perspective, applications of magnetoelectrochemistry have been in: electrodeposition of metals, conducting polymers, stripping voltammetry and microfluidics, which have been designed mostly around magnetohydrodynamic (MHD) convection caused by $\vec{F}_B$.[8-15] The direction of the magnetic field with respect to the electrode surface modifies nucleation versus growth resulting in different morphologies for electrodeposited metal films, which in some cases enhances their corrosion-resistance properties.[11] The primary effect through MHD is convection that increases the rate of mass transfer, and thus the deposition rate. Similarly, magnetic fields exert control over electropolymerization in terms of molecular weights, molecular ordering, film morphology/roughness and current efficiency.[16-39] MHD stirring during stripping voltammetry decreases the deposition time and enhances the stripping peaks, therefore increasing the detection limit of the method.[40-50] In microfluidics, electrochemical MHD can be considered as an almost intuitive extension of analogous action in liquid metals (e.g., MHD circulation of liquid sodium used for cooling of nuclear reactors[51,52]) and ionized gases.[53] Specifically, MHD has been used for pumping, mixing and separation. Using magnetic fields to control fluid flow on lab-on-a-chip devices circumvents the complexity of pumping with mechanical means, and the direction of flow can be reversed by simply changing the direction of the current (i.e., swapping the cathode for the anode) allowing for further miniaturization that increases portability, reducing fabrication costs as well as waste generation, and shortening analysis times.[54-67]

Understanding how to implement and control electrochemical magneto-hydrodynamics in micro and milli cells to perform pumping, mixing, and separating fluids has been explored but mainly through experiments.[68] Since current is what drives electrochemistry, experiments have been mostly on current measurement, however, in magnetohydrodynamics velocity measurements will provide further insight. The problem lies in the fact that in micro and milli electrode cells, while it is easy to measure current it is difficult to measure velocity accurately. Using dyes or colored redox radicals the macroscopic flow of the fluid can be tracked but cannot give a microscopic description of the flow. Fritsch et al. have used microbeads in channels to measure velocity.[70-72] Bead size, number density of beads, buoyancy and out of plane bead motion introduce errors into such measurements.

Simulations to aid in the understanding of the electrochemical magneto-hydrodynamic problem have been completed in the past. Work done by Sen et al. showed that a numerical approach could describe the electrochemical magneto-hydrodynamic problem fully.[73] The simulations also showed that a two-dimensional approach is appropriate for long channels where end effects of the channels are not significant. Three-dimensional simulations would be necessary if all the features of the problem cannot be captured using two-dimensional simulations.

Despite the sustained activity in the area by which the hydrodynamic problem and the electrochemical problem by themselves are well understood; the coupling of the two (and therefore the parameters that control electrochemical MHD) has been described only semi-quantitatively at best. In contrast to other well-known convective electrochemical systems, such as the rotating electrode or the jet-wall electrode where the electrochemical and hydrodynamic problems are not coupled via electrochemical reactions, the electrochemical MHD problem is described by a system of non-linear partial differential equations. Boundary conditions for the chemical species equation involved in the electrochemical reactions are also coupled making the problem intractable analytically. Willner et al. provided a 1 dimensional derivation of the limiting current and claims the equation takes the form of:

$$i_{l-MHD} \approx KA^{5/6} D^{8/9} \nu^{-2/9} \left(nC^*\right)^{4/3} B^{1/3} \qquad (4)$$

where $K = 0.63\pi^{1/6} F^{4/3} \rho^{-1/3}$, ρ is the density, $F$ is Faraday's constant, $A$ the surface area of the electrode ($cm^2$), $B$ the magnetic field strength (Tesla), $C_{bulk}$ the bulk concentration of the redox species (mol $cm^{-3}$), $D$ its diffusion coefficient ($cm^2$ $s^{-1}$), $\nu$ the kinematic viscosity of the electrolyte ($cm^2$ $s^{-1}$) and $n$ the number of electrons involved in the redox reaction. This equation is only valid for obtaining qualitative information on what the exponents are required to be, not to predict what the limiting current will experimentally be. This 1 dimensional derivation compliments the experimental work done by Leventis et al. in the presence of a uniform magnetic field without a paramagnetic redox species present in the solution.[refs]

Experimentally on the other hand, finding limiting current for the MHD problem (without a paramagnetic redox species) has been addressed independently by White and

Leventis from two opposite perspectives: with magnetic fields perpendicular to *micro*electrodes by White, and fields parallel to *milli*electrodes by Leventis (Figure 1). Numerical simulations of electrochemical MHD problem provide unique advantages, and recent two-dimensional simulations show their potential.[73,74]

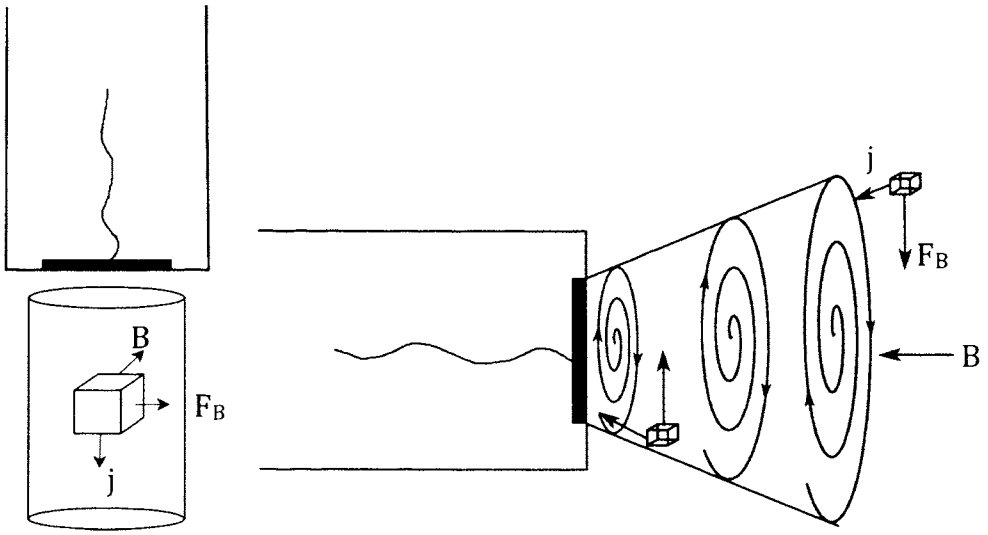


Figure 1: Schematic of the Lorentz effect. The left depitcs an experimental setup with the magnetic field parallel to the surface of the electrode; the direction of current flow and the magnetic field direction which inturn causes the Lorentz force. The right shows an experimental setup and the cyclonic flow patterns the accompny a magnetic field oreientation that is perpendicular to the working electrode. Also shown here is the direction of current flow, magnetic field, and Lorentz force.

White's experiments generates well-documented cyclonic flows.[68] However, owing to their use of small area electrodes, generation of large currents and therefore observable MHD phenomena required high concentrations of redox-active species. Consequently, the resulting steady-state voltammetric currents have contributions from both natural and MHD convection, which are difficult to deconvolute quantitatively.

On the other hand, Leventis' use of larger electrodes has allowed experimentation with low concentrations of redox-active species, and the dramatic change from a Randles-Sevcik peak-wave response to sigmoidal steady-state voltammetry has confirmed a magnetic field induced transition from diffusion-to-convention controlled mode of mass transfer. This is similar to current potential characteristics generated by rotating electrodes at ~100 rpm, where natural convention effects have less of an effect on the system. Subsequently, using a rigorous description of the magnetoelectrochemical problem, system parameters that should control MHD-limited currents, $i_{l\text{-}MHD}$, were identified and varied systematically, resulting in the semi-empirical expression, eq 5,

$$i_{l-MHD} = 4.31*10^{3} F A^{3/4} B^{1/3} C_{bulk}^{4/3} D \nu^{-1/4} n^{3/2} \quad (5)$$

where $F$ is Faraday's constant, $A$ the surface area of the electrode ($cm^2$), $B$ the magnetic field strength (Tesla), $C_{bulk}$ the bulk concentration of the redox species (mol $cm^{-3}$), $D$ its diffusion coefficient ($cm^2$ $s^{-1}$), $\nu$ the kinematic viscosity of the electrolyte ($cm^2$ $s^{-1}$) and $n$ the number of electrons involved in the redox reaction.[54]

A thorough examination of eq 5 is needed with the magnetic field oriented both parallel and perpendicular to the electrode surface. Experiments performed by Leventis and White are chosen for this.

The parallel case will be similar to Leventis' experimental setup and the perpendicular case follows White's experimental setup. Many factors are considered in the choice of experiments including: electrode size, magnetic field orientation, redox species, concentration of redox species, electrochemical cell size, and geometry are just a few. The numerical simulation here predicts accurate voltammograms and can capture the flow generated by the MHD body forces that are so strongly coupled to both the electrochemistry and hydrodynamics which proves, not only a set of equations that fully define the problem with boundary conditions, but also that a numerical simulation can be used as a design tool to predict various system characteristics. In a general way eq 5 will be interrogated with unknown coefficients:

$$i_{l-MHD} = (const.) F A^{a} B^{b} C_{bulk}^{c} D^{d} \nu^{e} n^{f} \quad (6)$$

In the parallel case we have been able to capture quantitatively the diffusion-to-convection transition in the shape of the voltammograms; experimental MHD-limited currents are reproduced within experimental error and eq 6 is validated fully by varying all parameters systematically. In the perpendicular case we have been able to reproduce qualitatively limiting currents in the absence and presence of the magnetic field, and to generate the observed convection patterns. As expected, the velocity field is influenced greatly by higher current densities, leading to larger $\vec{F}_B$ forces acting on volume elements close to the smaller (working) electrode.

Not discussed here are topics of eq's 2 and 3 and limiting currents that are a result of eq's 2 and 3.

## Theory and Simulation

### I. Governing Equations

To fully describe the Electrochemical Magnetohydrodynamics coupled problem the following set of equations must be solved as a coupled system:

$$\nabla \bullet \vec{V} = 0 \tag{7}$$

$$\rho \frac{D\vec{V}}{Dt} = -\nabla P + \mu \nabla^2 \vec{V} + \vec{j} \times \vec{B} + \rho \vec{g} \tag{8}$$

$$\frac{\partial C_m}{\partial t} = D_m \nabla^2 C_m - \vec{V} \nabla C_m \tag{9}$$

The derivations for these equations above can be found in supporting information, but these are the necessary equations that the simulation must solve. First conservation of mass for an incompressible fluid, conservation of momentum modified by the Lorentz force and finally Fick's second law modified by Nernst-Plank (without the migration term). Noting that the gravity term, $\rho \boldsymbol{g}$, causes natural convection to arise due to variations in density for the purposes of the present simulations density, $\rho$, is considered constant and the Boussineq approximation is not invoked.

Under this formulation, when a reaction occurs at the working electrode the model does not account for the fact that, to preserve charge neutrality, solvent molecules of density different from that of the redox species must be present. Since the solvent is part of the system, it causes natural convection to occur. For a case where the redox species is very dilute this is insignificant and the limiting current is mostly unaffected, but for the cases where there is a significant amount of redox species present natural convection plays a major role in the limiting current. Therefore only qualitative agreement was found for the parallel case.

### II. Initial Conditions

Since there is no inflow or outflow, the velocity of the fluid is initially zero. Applying a voltage to the electrodes causes Faradaic current to flow via the redox reaction, and the fluid is set in motion by the Lorentz force.

Initially the concentration of all constituents is known therefore this serves as the initial condition for concentration for the species equation.

**III. Boundary Conditions**

At every surface, including the working electrode, the no-slip condition is applied. This means that velocity at the surface is zero. The velocity normal to the surface is zero unless there is flow through that surface as in a porous media. The no-slip condition arises from the fact that viscosity causes the tangential velocity to be zero as well. Reynolds number is a useful non-dimensional parameter that can be used to describe flow regimes

$$\mathrm{Re} = \frac{\rho V D_h}{\mu} \quad . \tag{10}$$

For the largest velocity given by the parallel case the Reynolds number is, $\mathrm{Re} \sim .013$ which is $<<1$. Since the Reynolds number is so low the entire domain influenced by viscosity. It is noted, that these boundary conditions are general and allow any shaped domain to be considered without the need for a new set of hydrodynamic boundary conditions for other specific geometries (vessels). Regarding pressure, $P$, because of the small size of the electrochemical cell, and since the problem is treated as isothermal the pressure inside the entire domain is assumed to be constant. Note that the pressure gradient term in eq 8 will be zero for constant pressure. The solution is obtained using a reference pressure of 1 atm.

The boundary condition at the working electrode must contain the balance of species flux which is represented below

$$D_O \nabla C_O \big|_{at\_the\_electrode} = D_R \nabla C_R \big|_{at\_the\_electrode} . \tag{11}$$

This equation allows the formulation of current on the working electrode

$$\vec{i} = -nFAD_m (\nabla \cdot C_m)\big|_{normal\ \ to\ \ the\ \ electrode} \tag{12}$$

noting that this is total current on the working electrode. Our simulations give better resolution than this and current is known at all locations which allows the plotting of current spatially on the electrode surface.

In order to solve the species equation we invoked the Butler-Volmer formulation with the understanding that for facile electrode kinetics the Butler-Volmer equations will reduce to the Nernst equation. In order to control the reaction and carry out cyclic voltammetry we controlled the amount of voltage via

$$k_f = k^0 \, e^{\frac{-\alpha n F \eta}{RT}}$$
$$k_b = k^0 \, e^{\frac{(1-\alpha) n F \eta}{RT}} \quad (13)$$

where η is the overpotential, $k^0$ is the standard rate constant of eq 13, $\alpha$ the charge transfer coefficient ($0 \leq a \leq 1$), $E^{o'}$ the formal potential of the redox couple, and $R$ the universal gas constant. For our purposes, using *N,N,N′,N′*-tetramethyl-p-phenylene diamine as the redox active substance, $k^0$ was set at 0.55 cm $s^{-1}$, and $\alpha$=0.5 as reported by Compton.[69] The same $k^0$ and $\alpha$ were used for nitrobenzene as these would only skew/stretch the voltammograms for the parallel cases but would not affect the limiting current in an appreciable way. The reaction rates are then dictated by this overpotential which is linearly stepped between two values of voltage. The step size of the overpotential will be the sweep rate at which the experimental cyclic voltammetry was performed.

Numerical simulations of cells have been performed in the past. These simulations have comprised of 2D geometries which served as a starting point for the evaluation of the mathematical formulation herein. The 2D analysis is useful when examining the behavior in a long channel and a middle section of the channel were to be analyzed.76,77 The 2D model assumes that the flow will be unaffected in the third orthogonal direction which is not accurate for a small container with edge effects. We have taken this one step further and performed the simulation in 3 dimensions. This will allow for the capture of 3D vortices as well as other flow characteristics that occur only in 3 dimensions.

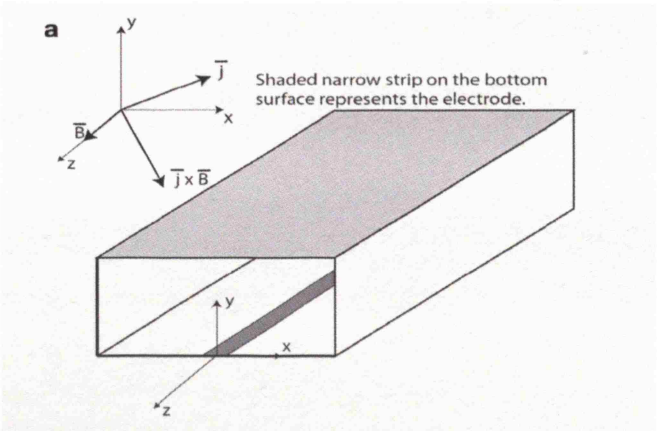


Figure 2: A representation of an extruded 2D simulation by Sen et al. A microstrip electrode is shown, that if the solution extended into ±∞ in the z-direction then a 2D slice may be taken. This means that there will be no flow in the z-direction, which is an estimation of reality.

In order to solve this highly coupled problem we employed the FLUENT® software package (a product of ANSYS®) in combination with user-developed code referred to as User-Defined-Functions (UDF's) coded in C for this problem.[75] Specifically, UDF's were written in order to: perform linear sweep and cyclic voltammetry, calculate the source term ($\vec{j} \times \vec{B}$), calculate the Arrhenius rate at each potential, calculate forward and backward reaction rates, calculate and store the concentration gradient, integrate and output electrode current. The calculation steps can be seen in Figure 3 which lays out the flow of the calculations and shows where the UDF's are implemented.[78,79]

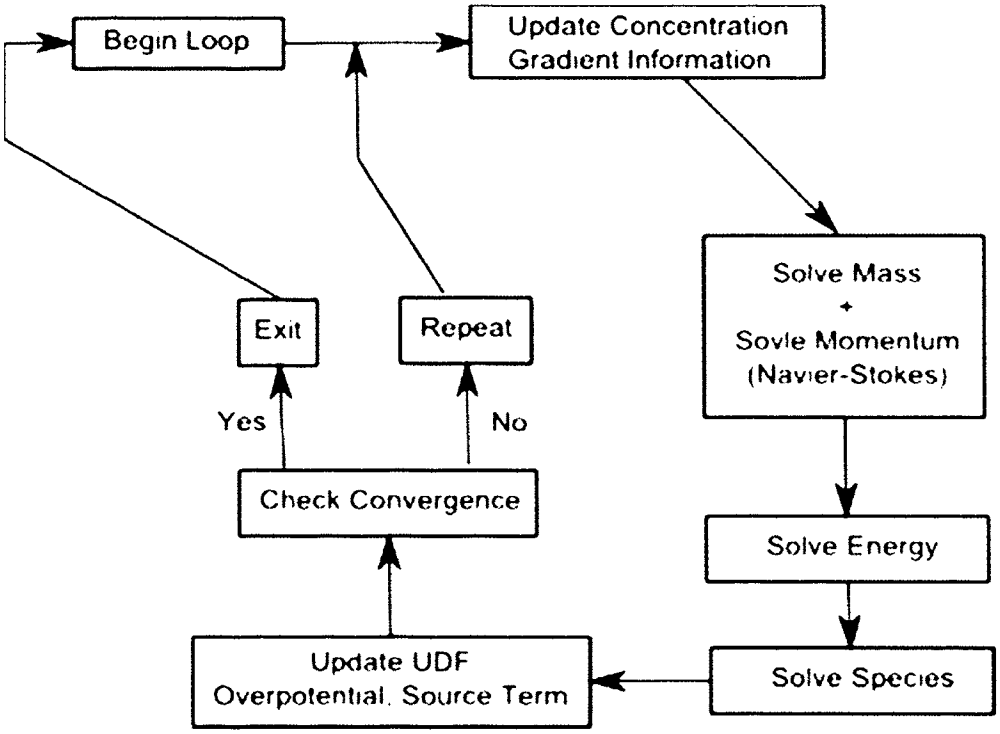


Figure 3: The flow diagram of the iteration process. The iteration begins with updating the concentraion gradient information from the UDF, then FLUENT® solves the mass, momentum, energy, and species equations. Next the UDF for linear voltammatry is updated as well as the source term for the Navier-Stokes equation. Lastly, convergence is checked and the loop is repeated as nessecary.

The linear sweep algorithm stepped the voltage applied to the Butler-Volmer equation and changed the energy barrier according to the new voltage (eq 13).

Calculating the electrode current is done by UDF. This was done using eq 14

$$i = \int_{electrode} nFD\left(\nabla \bullet C_{cell}\right) dA \qquad (14)$$

where $i$ is the total current on the working electrode, $n$ is the number of electrons participating in the reaction, $F$ is Faraday's constant, $D$ is the diffusion coefficient of either species.

The order in which this integration is performed numerically is by realizing that $n$, $F$, and $D$ are all constants and therefore can be pulled outside of the integral. Next, the UDF will sweep across the cells on the working electrode and at every cell it will calculate the area of that cell and the concentration gradient for that cell. It will then sum up all of these discrete cell values and then multiply by $n$, $F$, and $D$ to obtain the integrated current on the working electrode. This means that at every point (or cell) on the working electrode, a current, $i$, value is associated with that cell. Moreover, since the current is calculated for every point on the electrode this data is now available, and the surface of the working electrode can then be "probed" as in White's paper.

The source term $\vec{j} \times \vec{B}$ is calculated in a similar manner, but instead of integrating current over the surface of the working electrode the concentration gradient is found. Then the concentration gradient is multiplied by $n$, $F$, $D$, respectively and the cross product of B then applied as a body force in the Navier-Stokes equation.

Owing to the computation constraints, the geometry of the cell (Figure 1) was constructed by reducing the total volume of the electrochemical cells used in the respective experiments, but keeping the diameter of the disk working electrodes as the values reported (1.6 mm and 0.250 mm, respectively). In both cases the geometry of the electrochemical cell was axis-symmetric, with the counter electrode (10 times in diameter of the working electrode) comprising the entire bottom of the cylinder at a distance equal to 5 times the diameter of the working electrode and facing up towards the latter.

Using ANSYS® ICEM CFD™, a meshing software included in the ANSYS® CFD package, the space of the cylindrical cell was filled with an unstructured tetrahedral mesh. An unstructured mesh conforms to odd-shaped domains and allows for the size of the cells to vary more dramatically thus reducing the total number of cells needed. Use of a structured mesh was also attempted, but failed to allow the geometric flexibility needed to create a mesh having the required properties for good solution convergence.[80] In other words, the structured mesh diverged with the variation in some system parameters in which a new mesh was needed for the particular parameter. The mesh was finer near the

working electrode (at the top of the cylinder), growing progressively coarser towards the counter electrode (Figure 4), more can be found on the mesh setup in the supporting information.

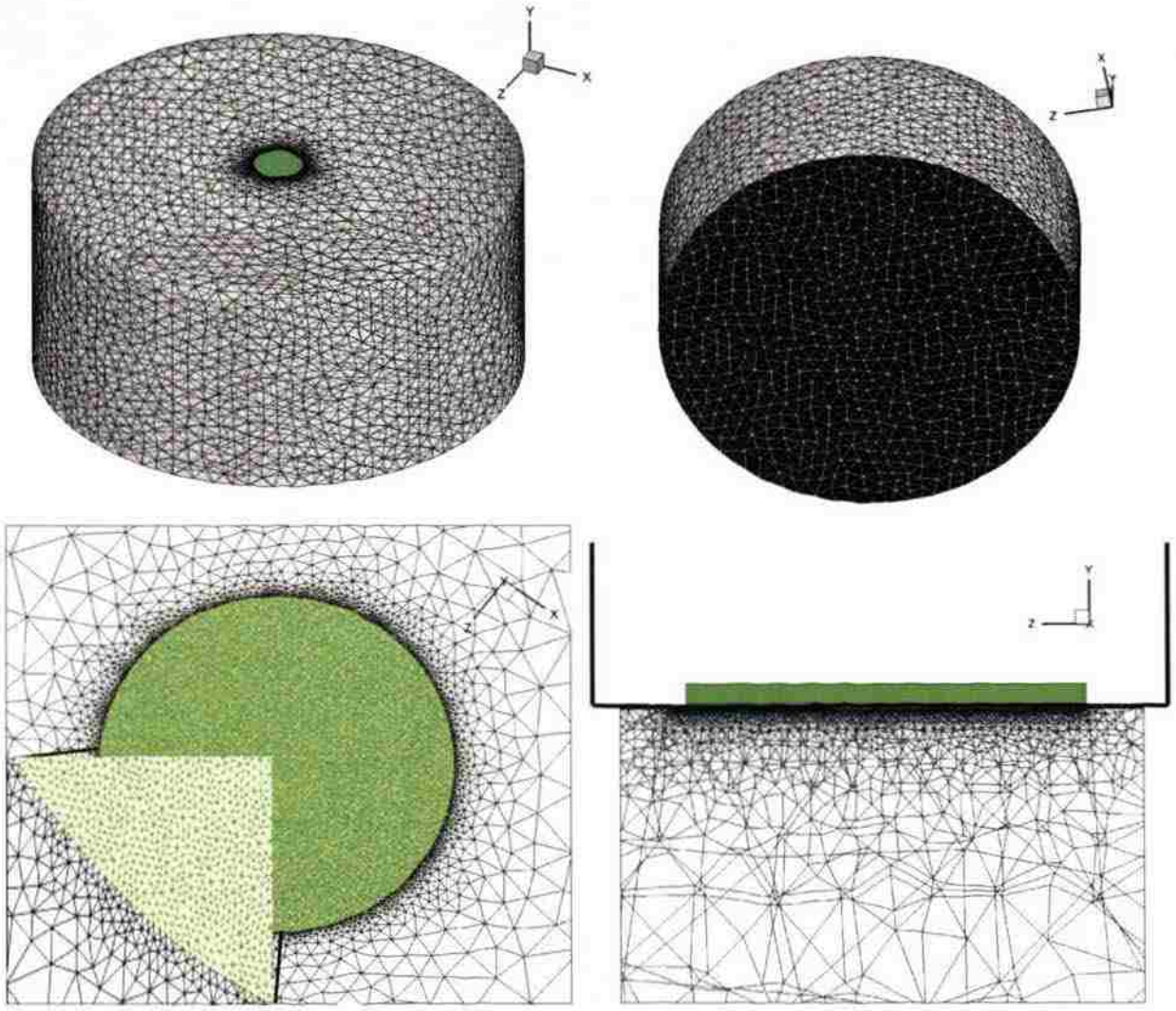

Figure 4: Mesh generation of computation cell. Top left displays the outside of the domain and overall surface mesh; the green solid circle is the working electrode. Top right shows the bottom of the domain where the counter electrode (black) is shown with it's surface mesh. Bottom left shows a top view of the working electrode and the progression of cells away from it. Bottom right is a side view of the working electrode as a cut plane of half the working electrode. This view depicts the transition of the mesh into the fluid growing coarser away from the working electrode.

**Case Setup**

In order to implement the numerical simulation the following information is needed: scaling factor of geometry, gravity, magnetic field strength and orientation, concentration of all species (concentration must be converted into mass fractions), viscosity of all species, diffusion coefficients, densities, $k^0$, starting and ending voltage to be swept, sweep rate, number of electrons, and molecular weights. With this information a transient solution can be attained.

To preserve consistency in running several simulations while varying a multitude of parameters a script was written to aid in the case setup process. This script utilized FLUENT's Text-User-Interface (TUI) in order to give commands to FLUENT. This was written in text format with comments on every line that describes what was changed. This allowed for a visual and easy way to change parameters in FLUENT and can also be used as conclusive evidence that on a case-by-case permutation the case setup was done the exact same way in the exact same order.

A transient second order accuracy coupled scheme was selected, meaning that the descretized time component will be of second order accuracy and the momentum equations will be coupled to the energy/species equations. Gravity is applied in the negative y-direction (normal to the working electrode) for the parallel cases, but not applied in the parallel cases. The reason to not include gravity in the parallel cases is because the amount of convection that is generated in the non-MHD case. This changes the current numbers enough in the parallel case to cause confusion (more will be discussed on this later).

The convergence criteria were left as default values, except for oxidized and reduced species, in which the convergence criteria needed to be stricter therefore a residual of $1e^{-6}$ was used.

All UDF's were written and compiled utilizing Microsoft Visual Studio 2010®. The simulations were run on a High-Performance Cluster in which each node contains 12 CPU cores (Intel X5680 3.33GHz) and 96 GB RAM (1333 MHz) and was provided by Dr. Richard Dawes (MS&T Chemistry). In which it would take approximately 7-14 days to run a Cyclic Voltammagram of an MHD simulation at a sweep rate of $\nu$=10 mV/s.

**Results and Discussion**

System parameters were systematically varied for the parallel case setup, the simulation must first be validated. This is done by showing that varying only the sweep rate while keeping all other parameters constant reproduces the same limiting current.

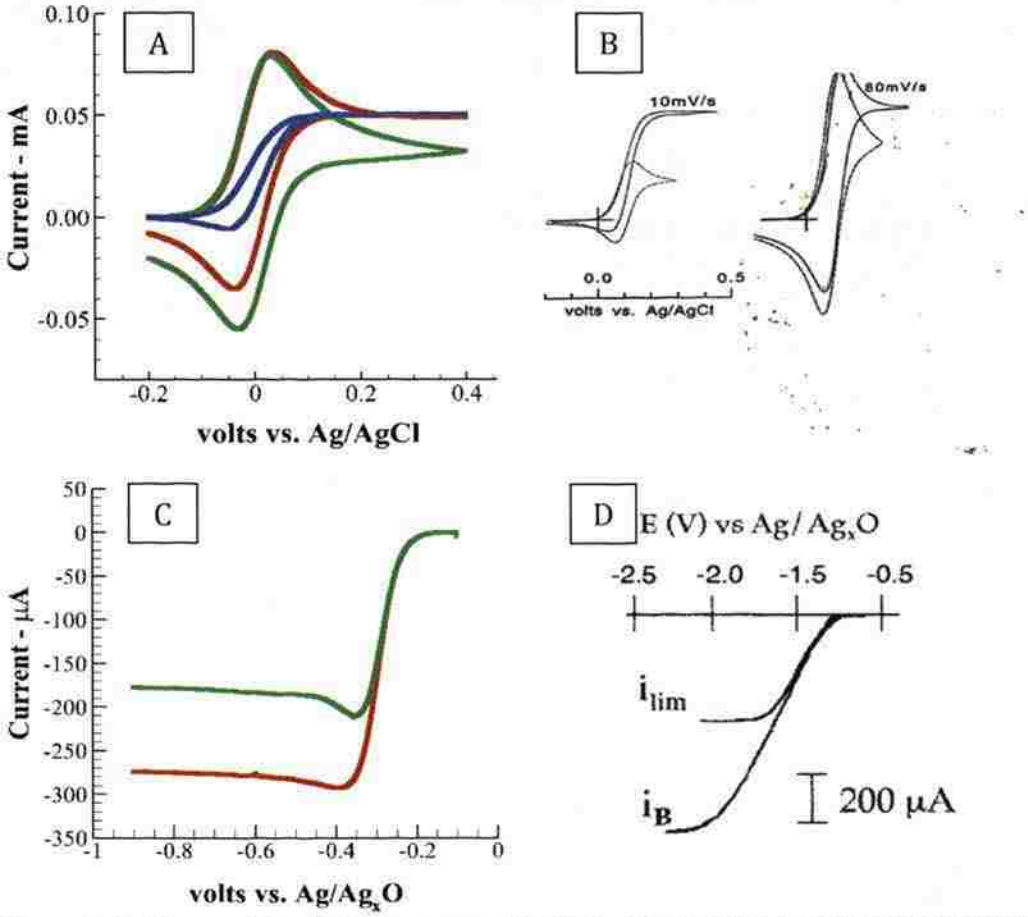


Figure 5: Evidence of simulation accuracy. A) 10.26mM of TMPD in $CH_3CN$/0.5M TBAP; the blue line has a sweep rate of 10 mV/s and a magnetic field of B = 1.75. The red line has a sweep rate of 80 mV/s with B = 1.75 and the green line has a sweep rate of 80 mV/s but B = 0 (no MHD effects). B) Shows experimental data for 10.89mM concentration of TMPD $CH_3CN$/0.5M TBAP. C) shows simulation data for the parallel case with cyclonic flow in 0.5M NB $CH_3CN$/0.5M TBAP. D) The experimental data of 0.5M NB in $CH_3CN$/0.5M TBAP.

In Figure 5A the blue line shows no diffusional wave and is completely mass transfer controlled for the forward sweep but on the reverse sweep a small diffusional wave is present. The diffusional wave on the reverse sweep is due to the recovering of reduced species still in the solution whereas the forward sweep will contain no oxidized species to recover thus a small diffusional wave does not appear. The limiting current for the experiment was approximately 0.05mA and the limiting current for the simulation was 0.0504 mA matching within experimental error. The green line in Figure 5A shows that if

no magnetic field is present then there will not be an enhancement of the current and in fact a steady-state current does not exist. Figure 5 C shows the simulation result with the magnetic field oriented as in Figure 1B shows. Here cyclonic flow is generated which in the presence of a magnetic field still enhances limiting current. In this system a large portion of the solution is redox species and therefore generates a large amount of natural convection that is not yet captured by the simulations.

Since accurate limiting currents are obtained in the parallel case the velocity field setup by the Lorentz force causes fluid to be displaced from the working electrode. In Figure 6A the simulation shows that the concentration of TMPD being displaced as in the photo of the experiment in Figure 6B which shows that the velocity field created matches the experimental velocity field near the working electrode. Figure 6C shows the streamlines if the magnetic field is oriented as in Figure 1B. The streamlines are shown and the cyclonic flow is observed. The coloring of the streamlines indicates the concentration of the redox species; red being the reduction of NB at the electrode and fading through the colors to blue. Here the inner part of the vortex can be seen which follows the experimental data exactly. Since the counter electrode is simply there to complete the circuit when the vortex is formed the center of the vortex funnels solution directly to the working electrode.

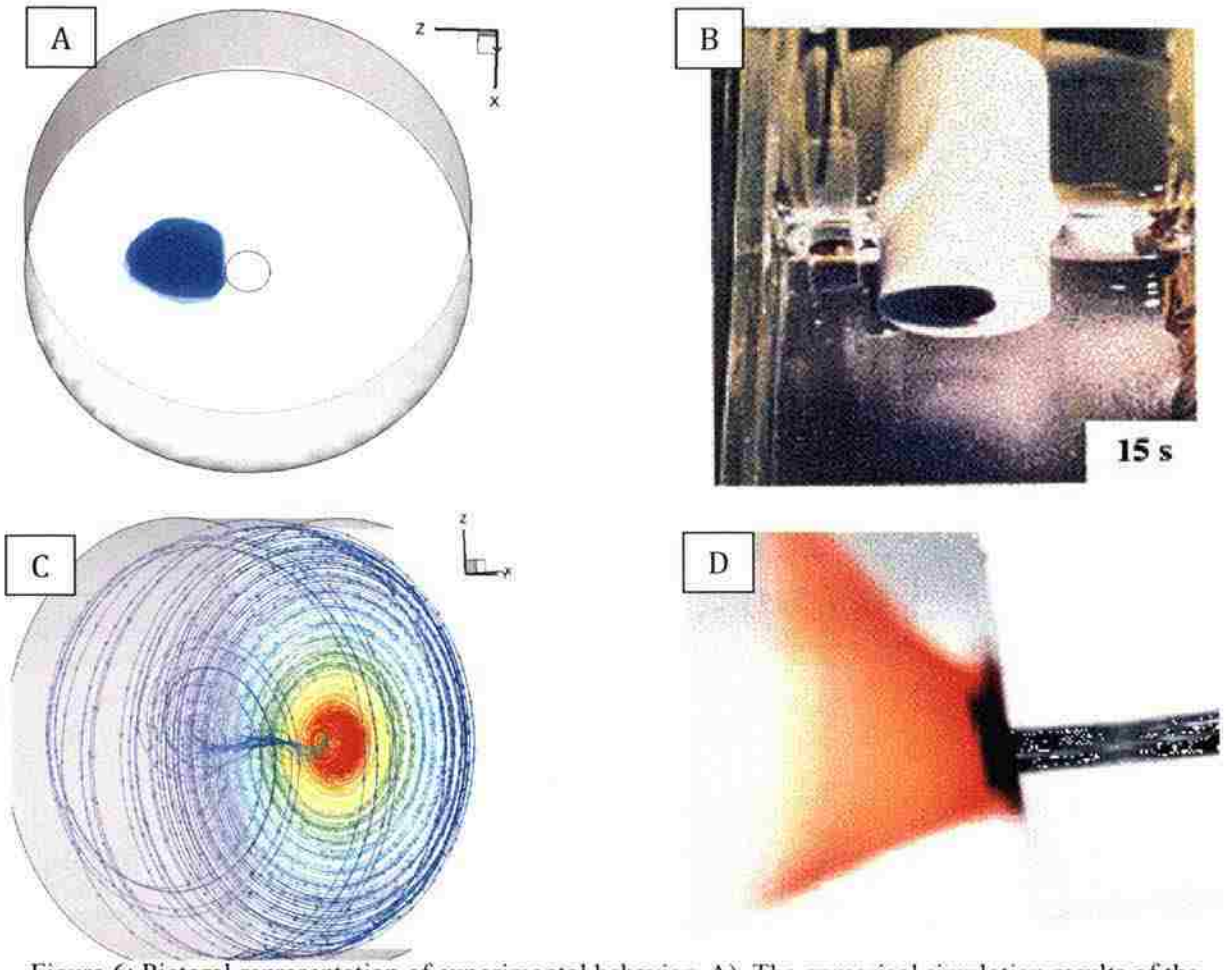


Figure 6: Pictoral representation of experimental behavior. A) The numerical simulation results of the parallel case where the contours of TMPD can be seen and illistrates the Lorentz force in the correct direction, which matches the experiment in B. C) Shows the numerical simulation streamlines where the coloring of the streamlines shows the concentration of NB, and the direction of the streamlines confirms the cyclonic flow of the experiment in D.

Now knowing that the simulation can provide accurate limiting current and flow patterns we varied all of the system parameters in eq 6 in order to obtain the exponents.

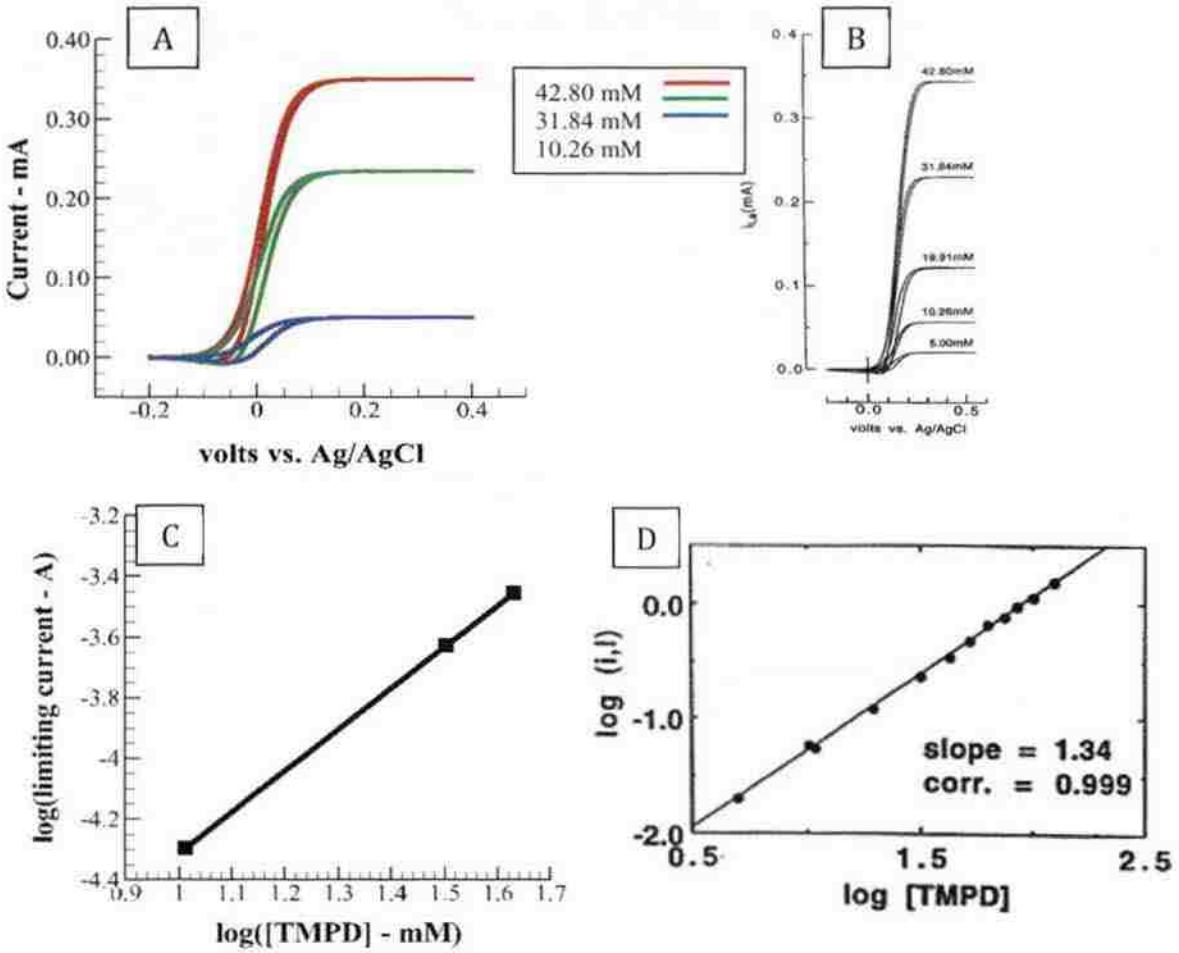


Figure 7: Varying concentration. A) Shows the simulation cyclic voltammagrams at a sweep rate of 10mV/s. The limiting current was then plotted in C which makes a straight line with slope 1.35 confirming the slope to be 4/3. B) shows the experimental cyclic voltammagrams which match the simulation, and D is the experiment data plotted with a slope of 1.34.

Concentration was varied from as shown in Figure 7A and the limiting currents are plotted in Figure 7C. The limiting currents produced a slope of 1.35 and a $R^2$=1. This proves that the dependence on concentration in eq 6 is 4/3.

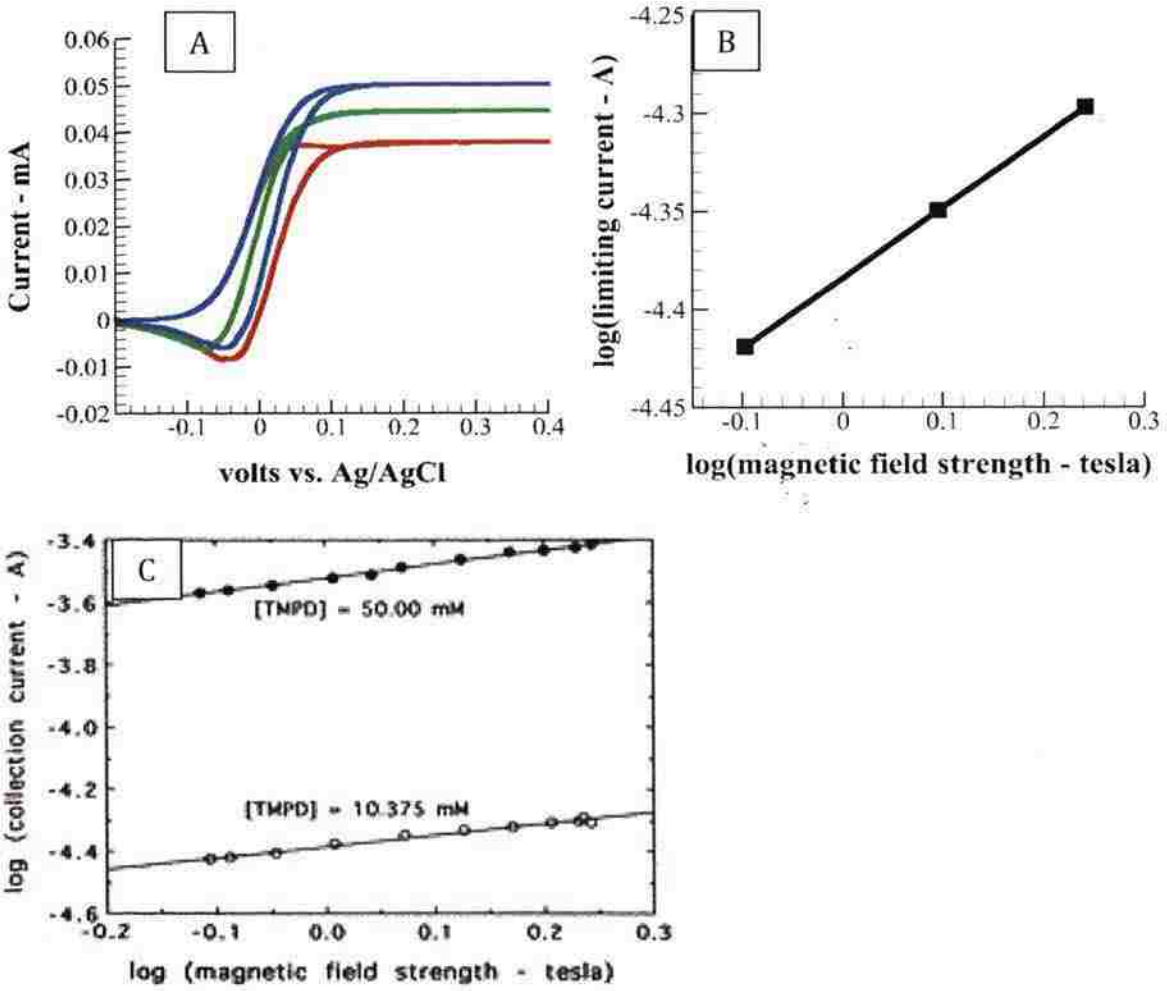


Figure 8: Varying magneic field. A) The simulated data that follows the pattern of C. The magnetic field was varied by: B = 0.8, 1.25, 1.75 which are colored red, green, and blue respectively. B) The slope of the simulated line is 0.35 which is within experimental error confirming an exponent of 1/3. C) The experimental data which shows a slope of 0.44 for 50.00mM and 0.36mM for 10.375mM.

Magnetic field was then varied and the cyclic voltammogram can be seen in Figure 8A in which the limiting currents are plotted and a slope of 0.35 was obtained with a $R^2$=1. This cofirms the exponent in eq 6 to be 1/3.

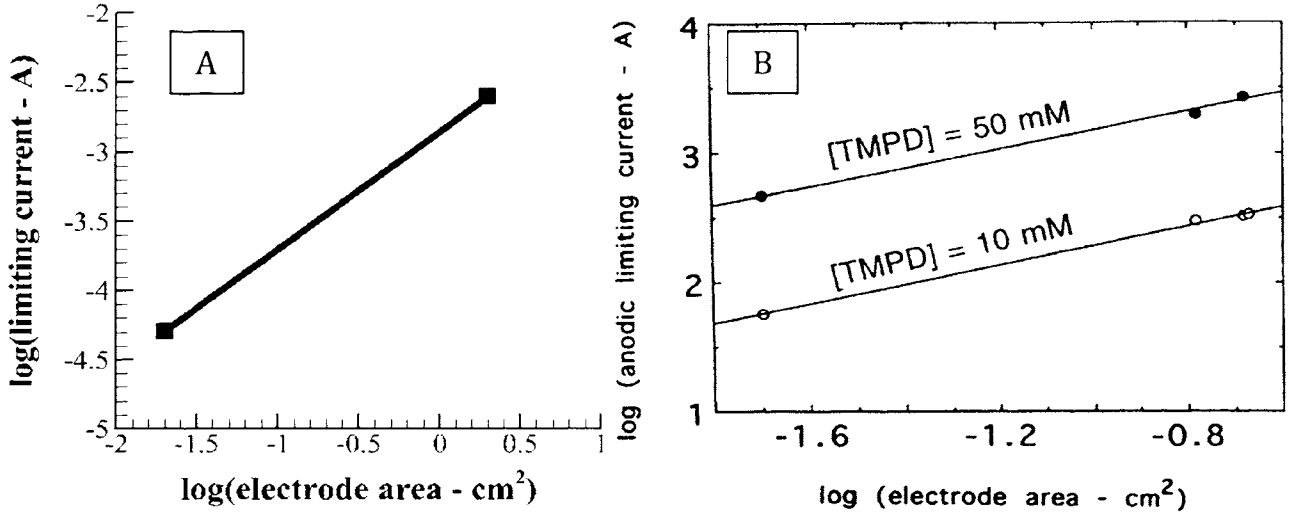


Figure 9: Varying eletrode area. A) The electrode area, which due to computation accuracy and overall run time only two data points were plotted. The area of the simulations were 0.0201cm$^2$ and 2.01cm$^2$ respectively which yielded a slope of 0.78. B) Shows the experimental data which contains a slope of 0.75 for both concentrations used.

Next the area was increased to a size that was not performed experimentally. The motive for this was if the electrode is instead made smaller then radial diffusion effects become more significant and this will influence the limiting current. The area was increased by two orders of magnitude which correlates to a diameter that is 400 times larger. This revealed a slope of 0.78 and a $R^2$=1. Confirmeing the exponent in eq 6 to be ¾.

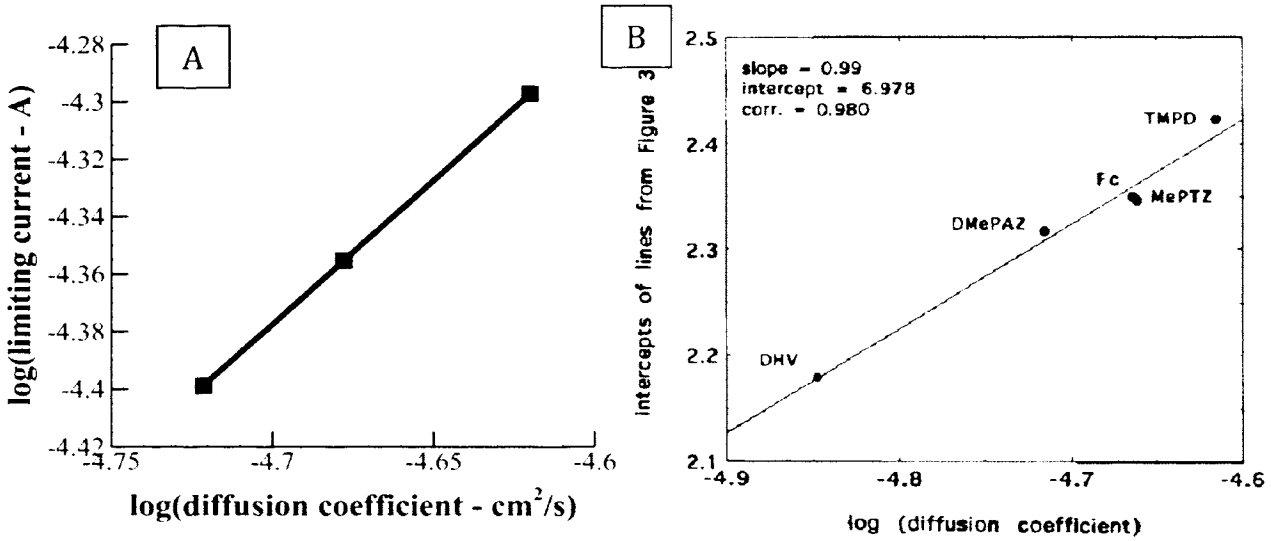


Figure 10: Varying diffusion coefficient. A) shows the simulation data for diffusion coefficients of D = 2.4e-9, 2.1e-9, 1.9e-9 m$^2$/s and yields a slope 1.00 confirming the experimental data in B.

Next diffusion coefficient was varied and the limiting current shows the slope to be 1.00 with a $R^2$=1 thus confirming eq 6 exponent to be 1.

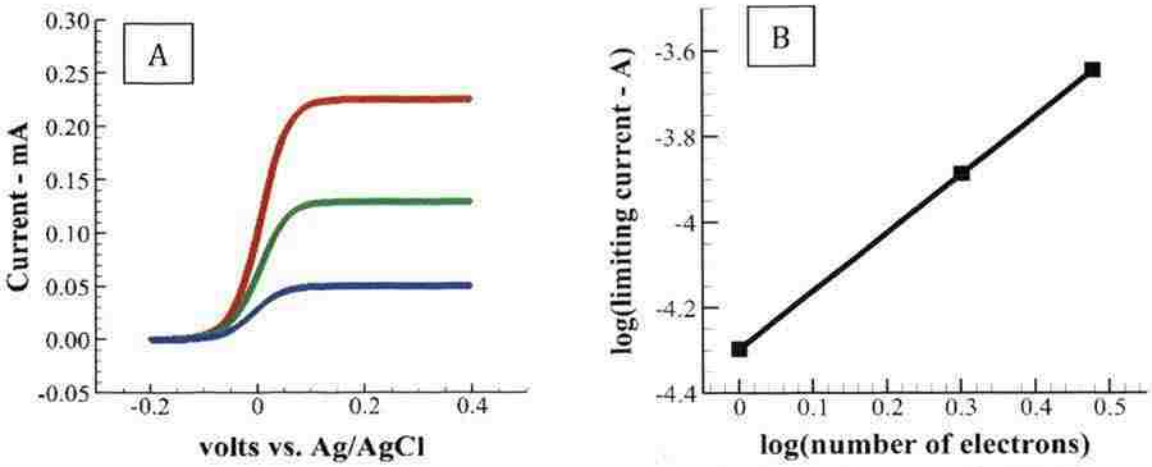


Figure 11: Varying the number of electrons. Performing only the forward sweep at 10mV/s. The numbers of electrons varied are n = 1, 2, 3 indicated by the blue, green, and red lines respectively.

The number of electrons transferred in the redox process was increased from 1 to 2 and 3. In the simulation we do not provide a mechanism to have the reaction take place as it does in experiments. Instead the simulation releases 2 or 3 electrons for every redox reaction. This is not how the reaction takes place experimentally but should be close enough to give the proper limiting currents. In previous work several methods have been employed to scale the results of the experiment to obtain accurate results. Here the simulation can calculate the limiting current without the need for scaling. Previously the exponent on the number of electrons was thought to be 3/2 but here the simulation predicts the slope and therefore exponent to be 4/3 and a $R^2$=1. Since the simulation is using first order data not derived data or data that have been scaled and the accuracy of the simulation thus far has been proven, we believe the exponent to be 4/3 and not 3/2 which is in agreement with Willner et al.

Noting that kinematic viscosity is absolute viscosity divided by density, caution must be given here as previous equations have fallen sort of describing the relationship between these two. Willner et al. touched on the matter but put $\rho^{-1/3}$ in the constant, thus washing out its effects. Pulling density out of the constant and separating the kinematic viscosity then the total dependence on density is to the -1/9 power, and absolute viscosity to the -2/9 power. Leventis et al. falls sort of quantifying the dependence of density and viscosity independently and instead only considers kinematic viscosity. Here through simulation we have obtained the dependence on viscosity and density independently. This

was done by graphing in 3D the viscosity, density and limiting current divided by all the system parameters as shown in Figure 12.

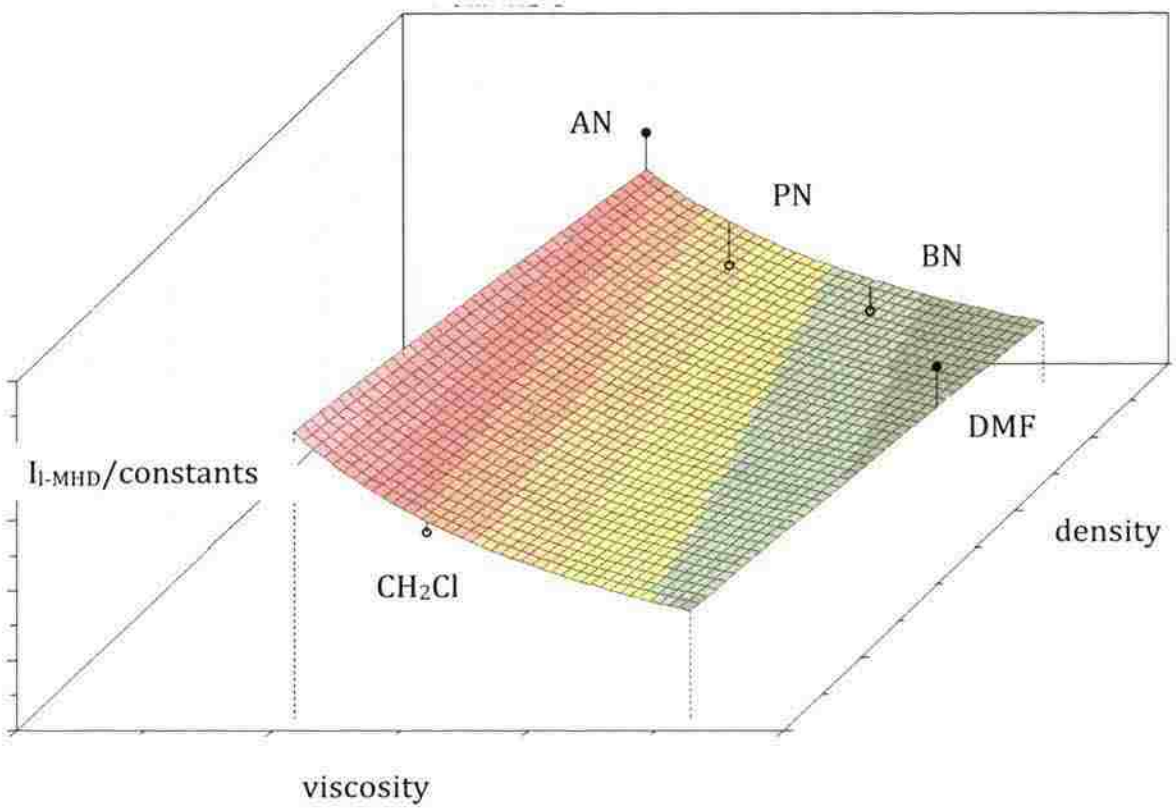


Figure 12: All experimental data plotted in a 3D graph. The $R^2$yy(x)=0.71. Exponents for viscosity is -0.46 and 0.36 for density.

The uncertainty in the 3D graph is mainly attributed to only comparing 5 data points. The final form of the simulated general equation is:

$$i_{l-MHD} = 4.31*10^3 FA^{3/4} B^{1/3} C_{bulk}^{4/3} D\mu^{-1/2} \rho^{1/3} n^{4/3} \quad (15)$$

which is similar to previously stated equations but takes into account the separate effects of density and absolute viscosity.

**References**


1) Faraday, M. *Diary*; Bell and Sons: London, 1933; Vol. IV 288, pp 7706-21.

2) Coey, J. M. D.; Rhen, F. M. F.; Dunne, P.; Mc-Murry, S. J. *Solid State Electrochem.* **2007**, *11*, 711–717.

3) Leventis, N.; Dass, A. *J. Am. Chem. Soc.* **2005**, *127*, 4988–4989.

4) O'Brien, R. N.; Santhanam, K. S. V. *J. Appl. Electrochem.* **1990**, *20*, 427.

5) Ragsdale, S. R.; Grant, K. M.; White, H. S. *J. Am. Chem. Soc.* **1998**, *120*, 13461.

6) Grant, K. M.; Hennert, J. W.; White, H. *S. Electrochem. Commun.* **1999**, *1*, 319.

7) Hinds, G.; Coey, J. M. D.; Lyons, M. E. G. *Electrochem. Commun.* **2001**, 3, 215.

8) Fahidy T. Z. *J. Appl. Electrochem.* **1983,** *13*, 553.

9) Fahidy T. Z. *Prog. Surf. Sci.* **2001,** 68, 155

10) Dash, J.; King, W.W.; *J. Electrochem. Soc.* **1972,** *119*, 51.

11) Csokán, P.; Figy K. **1979,** *19*, 8 (in Hunarian).

12) Mohanta, S.; Fahidy, T.Z. *Can. J. Chem. Eng.* **1972,** *50*, 248.

13) Mohanta, S.; Fahidy, T.Z. *Electrochim. Actas*, **1974,** *19*, 771.

14) Ishmail, M.I.; Fahidy, T.Z. *Can. J. Chem. Eng.* **1979,** *57*, 734.

15) Ishmail, M.I.; Fahidy, T.Z. *Can. J. Chem. Eng.***1980,** *58*, 505.

16) Mohanta, S.; Fahidy, T.Z. *Can. o r. Chem. Eng.* **1972,** *50*, 248.

17) Bozorth, R.M. *Phys. Rev.* **1925,** *26*, 390.

18) Csokan, P.; Korroz. Figy. **1979**, *19*, 8.

19) Fahidy T. Z. *J. Appl. Electrochem.* **1983**, *13*, 553.

20) Bund A.; Ispas A.; Mutschke G.; *Sci. Technol. Adv. Mater.* **2008**, *9.*

21) Chiriac A.P.; Simionescu C.I. *Prog Polym Sci* **2000**, *25*, 219.

22) Landee C.P.; Melville D.; Miller J.S. *Magnetic molecular materials* **1990**, *198*, 395.

23) Chiriac AP, Simionescu CI (2000) *Prog Polym Sci* **2000,** *25*, 219.

24) Kaptein R.; Oosterhoff J.L. *Chem Phys Lett* **1969,** *4*, 195.

25) Closs G.L. *J Am Chem Soc* **1969**, *91*, 4552.

26) Chiriac A.P.; Simionescu C.I.; Neamtu I.; Popa M. (1998) *Cell Chem Technol* **1998,** *32*, 425.

27) Chiriac A.P.;, Neamtu I.;, Cazacu G.;, Simionescu C.I.;, Rozmarin G. *Angew Makromol Chem* ,**1997**,*246*,1.

28) Junlian H.; Wu Q. *Chin J Polym Sci* **1990,** *8*, 108.

29) Osawa S.; Ogawa T.; Ito M. *Synth Met* **1997,** *90*, 109.

30) Wan M.; Yang J. *Synth Met* **1995**, *69*, 155.

31) Cai L.T.; Yao S.B.; Zhou S.M. *J Electroanal Chem* **1997,** *421*, 45.

32) Inoue Y.; Yamato M.; Kimura T.; Ito E.; *Synth Met* **1997,** *84*, 435.

33) Mogi I.; Kamiko M. *J Cryst Growth* **1996,** *166*, 276.

34) Mogi I.; Kamiko M. *Bull Chem Soc Jpn* **1996** , *69*, 1889.

35) Leventis N.; Dass A.; Chandrasekaran N. *J. Solid State Electrochem.* **2007,** *11*, 727-735.

36) Woodson, H.H.; Melcher, J.R. *Electrome-2 chanical Dynamics.* **1969,** John Wiley, New York. Vol. 3.

37) Davidson, P.A.; *An Introduction to Magnetohydrodynamics* **2001,** Cambridge University Press, Cambridge.

38) Manz, A.; Graber, N.; Widmer, H. M. *Sens. Actuators, B: Chem.* **1990**, *1*, 244–248.

39) Qian S.; Bau H. *Mechanics Research Communications* **2009**, *36*, 10-21.

40) Richter, P.; Toral, M. I.; Abbott, B. *Electroanalysis* **2002**, *14*, 1288-1293.

41) Prakash, R.; Srivastava, R. C.; Seth, P. K. *Electroanalysis* **2001**, *14*, 303-308.

42) Emons, H.; Baade, A.; Schoning, M. *J. Electroanalysis* **2000**, *12*, 1171-1176.

43) Petrie, L. M.; Baier, R. W. *Anal. Chem.* **1978**, *50*, 351-357

44) Liu, T. Z.; Lai, D.; Osterloh, J. D. *Anal. Chem.* **1997**, *69*, 3539-3543.

45) Hardcastle, J. L.; Compton, R. G. *Electroanalysis* **2002**, *14*, 753-759.

46) West, C. E.; Hardcastle, J. L.; Compton, R. G. *Electroanalysis* **2002**, *14*,1470-1478.

47) Authier, L.; Grossiord, C.; Brossier, P. *Anal. Chem.* **2001**, *73*, 4450-4456.

48) Wang, J.; Liu, G.; Polsky, R.; Arben, M. *Electrochem. Comm.* **2002**, *4*, 722-726.

49) E. A. Clark and I. Fritsch, *Anal. Chem.*, **2004**, *76*, 2415.

50) E. C. Anderson and I. Fritsch, *Anal. Chem.*, **2006**, *78*, 3745.

51) Araseki H.; Kirillov I. R.; Preslitsky G.V. *Nuclear Engineering and Design*, **2011**

52) Araseki H.; Kirillov I. R.; Preslitsky G.V.; Ogorodnikov A. P. *Nuclear Engineering and Design*, **2004**, *227*, 29-50.

53) Spitzer L. *Physics of Fully Ionized Gases*, **1962** (2d ed.; New York;Interscience)

54) Leventis, N.; Chen, M.; Gao, X.; Canalas, M.; Zhang, P. *J. Phys. Chem. B* **1998**, *102*, 3512-3522.

55)Sadler, D. J.; Changrani, R. G.; Chou, C. F.; Daniel, Z.; Jeremy, W. B.; Frederic, Z. *Proc. SPIE*, **2001**, *4560*, 162-69.

(57) Bau, H. H.; Zhong, J.; Yi, M. *Sens. Actuators, B* **2001**, *79*, 207-215.

(58) Jang, J.; Lee, S. S. *Sens. Actuators, A*, **2002**, *80*, 84-89.

(59) Lemoff, A. V.; Lee, A. P. *Sens. Actuators, B* **2000**, *63*, 178-185.

(60) Lemoff, A. V.; Lee, A. P. *Biomed, Microdevices* **2003**, *5*, 55-60.

(61) West, J.; Karamata, B.; Lillis, B.; Gleeson, J. P.; Alderman, J. *Lab Chip* **2002**, *2*, 224-30.

(62) Leventis, N.; Gao, X. *J. Phys. Chem. B* **1999**, *103*, 5832-5840.

(63) Ragsdale, S. R.; Lee, J.; Gao, X.; White, H. S. *J. Phys. Chem.* **1996**, *100*, 5913-5922.

(64) Ragsdale, S. R.; Lee, J.; White, H. S. *Anal. Chem.* **1997**, *69*, 2070-2076.

(65) Lee, J.; Ragsdale, S. R.; Gao, X.; White, H. S. *J. Electroanal. Chem.* **1997**, *422*, 169-177.

(66) Aaboubi, O.; Chopart, J.P.; Douglade. J.; Olivier, A. *J. Electrochem. Soc.* **1990**, *137*, 1796-1804.

(67) Aaboubi, O.; Amblard; Chopart, J.P.; Olivier, A. *J. Electrochem. Soc.* **2003**, 150, E125-130.

(68) Pullins, M. D.; Grant, K. M.; White, H. S. *J. Phys. Chem. B* **2001**, *105*, 8989-8994.

(69)Clegg, A. D.; Rees, N. V.; Klymenko, O. V.; Coles, B. A.; Compton, R. G. *"Experimental Validation of Marcus Theory for Outer-Sphere Heterogeneous Electron-Transfer Reactions," ChemPhysChem*, *5*, 1234-1240.

(70) Melissa C. Weston, Matthew D. Gerner, and Ingrid Fritsch *Anal. Chem.* **2010,** *82,* 7068-7072.

(71)Cheah L.; Fritsch I.; Haswell S.; Greenman J. *Biotechnology and Bioengineering* **2012**, doi: 10.1002/bit.24426

(72) Melissa C. Weston, Matthew D. Gerner, and Ingrid Fritsch *Anal. Chem.* **2010,** *82,* 3411–3418.

(73) Sen D.; Isaac K. M.; Leventis N; Fritsch I. *International Journal of Heat and Mass Transfer* **2011**, *54*, 5368-5378.

(74) Qian S.; Bau H. *Physics of Fluids* **2005**, *17*, 067105.

(75) ANSYS FLUENT 12.1 Users Guide. https://www.sharcnet.ca/Software/Fluent12/pdf/wbug/flwb.pdf (accessed Feb 29, 2012).

(76) Sen D.; Isaac K.; Leventis N.; Fritsch I. *6th AIAA Theoretical Fluid Mechanics Conference* (Honolulu), Hawaii, June 27-30, 2011

(77) Sen D.; Isaac K.; Leventis N.; Fritsch I. *48th* Aerospace Sciences Meeting Including the New Horizons Forum and Aerospace Exposition (Orlando), Florida, January 4-7, 2010

(78) ANSYS FLUENT 12.0 UDF Manual. https://www.sharcnet.ca/Software/Fluent12/pdf/udf/fludf.pdf (accessed December 10, 2011).

(79) ANSYS FLUENT 12.0 Theory Guide. http://www1.ansys.com/customer/content/documentation/121/fluent/flth.pdf (accessed December 10, 2011).

(80)ICEM User Manual http://www1.ansys.com/customer/content/documentation/120/icemcfd/icmuser.pdf (accessed August 15, 2011).

# APPENDIX
# SUPPORTING INFORMATION

## S1 Derivation for Coupled System

The electrochemical cell consists of a redox species in electrolyte and platinum electrodes. Two cases are presented: first the parallel cases are chosen with TMPD and in $CH_3CN$/0.5M TBAP, second, perpendicular cases are modeled with 0.5M Nitrobenzene in $CH_3CN$/0.5M TBAP. Convection arising from the Lorentz force, $\vec{F}_B$, causes the electrolyte with redox species to be displaced. The momentum equation modified by the Lorentz force describes the relationship between applied forces on a unit volume element and the resulting motion is described by Newton's second law applied to continuum and referred to as the Navier-Stokes equation

$$\rho \frac{D\vec{V}}{Dt} = -\nabla P + \mu \nabla^2 \vec{V} + \vec{j} \times \vec{B} + \rho \vec{g} \tag{8}$$

where $\rho$ is the density of the electrolytic solution, $P$ the generalized pressure, $\mu$ the absolute viscosity, and $\vec{g}$ the acceleration of gravity. The material derivative $D/Dt$ includes the local temporal derivative $\left(\frac{\partial \vec{V}}{\partial t}\right)$ as well as the convective derivative $\left(\left(\vec{V} \cdot \nabla\right)\vec{V}\right)$ of the velocity vector. The gravity term, $\rho\vec{g}$, causes natural convection to arise due to variations in density. For the purposes of the present simulations density, $\rho$, is considered constant, and the Boussinesq approximation is not invoked. Under this formulation, when a reaction occurs at the working electrode the model does not account for the fact that, to preserve charge neutrality, solvent molecules of density different from that of the redox species must be present. Since the solvent is part of the system, it causes natural convection to occur. For the Leventis case this is insignificant as the redox species is extremely diluted and the limiting current is mostly unaffected, but for the White case natural convection plays a major role in the limiting current. Therefore only qualitative agreement was found for Whites case. The present simulations have highlighted the need for accurate measurement of the velocities for more detailed

comparison of the experiments and the simulations. The fluid is considered incompressible, therefore the continuity (mass conservation) equation dictates

$$\nabla \bullet \vec{V} = 0 \quad (7)$$

**S2 Electrochemistry Boundary and Initial Conditions**

The boundary conditions for the electrochemistry involves the ionic current density, $\vec{j}$, that drives the MHD stirring described above which is generated by redox reactions that take place at the surface of the working electrode

$$O + ne \rightleftarrows R \quad . \quad (S1)$$

The heterogeneous electron transfer is driven by the electrode potential, $E$, that sets the surface concentrations of species $O$ and $R$ according to the appropriate boundary conditions. Thus, the total electrolytic current, $\vec{i}$, flowing through the cell is controlled by the flux of species $O$ at the electrode, $\vec{J}_O$, i.e., by how fast species $O$ can be supplied to the electrode (eq 11), or equivalently, by how fast $R$ can be

$$\vec{i} = nFA\vec{J}_O\Big|_{normal\ \ to\ \ the\ \ electrode} \quad (S2)$$

removed, moderated by the kinetics of the heterogeneous electron transfer according to the current-potential characteristic (eq S3).

$$\vec{i} = AFk^o\left[C_O\Big|_{at\ \ electrode}\exp\left(-a\frac{nF}{\Re T}(E-E^{o'})\right)\right] - AFk^o\left[C_R\Big|_{at\ \ electrode}\exp\left((1-a)\frac{nF}{\Re T}(E-E^{o'})\right)\right] \quad (S3)$$

where $k^0$ is the standard rate constant of eq S3, $\alpha$ the charge transfer coefficient ( $0 \le a \le 1$ ), $E^{o'}$ the formal potential of the $O/R$ couple, and $\Re$ the universal gas constant. For our purposes, using $N,N,N',N'$-tetramethyl-p-phenylene diamine as the redox active substance, $k^0$ was set at 0.55 cm $s^{-1}$, and $\alpha$=0.5 as reported by Compton.[69] The same $k^0$ and $\alpha$ were used for nitrobenzene as these would only skew/stretch the voltammograms for Whites cases but would not affect the limiting current in an appreciable way.

In general, the flux $\vec{J}_m$ of any species $m$ is described by three additive components arising from diffusion, migration and convection, according to the Nernst-Plank equation (eq S4), where $D_m$ is the diffusion coefficient of species $m$, and $\nabla\phi$ the electrostatic

$$\vec{J}_m = -D_m \nabla C_m - \frac{z_m F}{\Re T} D_m C_m \nabla\phi + C_m \vec{V} \tag{S4}$$

potential gradient at the point of interest. It can be shown that in the presence of a large excess of supporting electrolyte, the migration component to the ionic current can be neglected, hence transport of $O$ or $R$ can be described adequately by diffusion and convection only. Therefore,

$$\vec{i} = nFAD_m[-\nabla \cdot C_m + \nabla \cdot (C_m \vec{V})]\Big|_{normal\ \ to\ \ the\ \ electrode} \tag{S5}$$

However, since at the electrode $\vec{V}\Big|_{at\ \ boundary} = 0$ (no-slip condition), eq S5 evolves into:

$$\vec{i} = -nFAD_m(\nabla \cdot C_m)\Big|_{normal\_to\_the\_electrode} \tag{S6}$$

To calculate the current, and hence the MHD force, we need to know the evolution of the concentration profiles, which is described by eq S6,

$$\frac{\partial C_m}{\partial t} = -\nabla \cdot \vec{J}_m \tag{S7}$$

and the Nernst-Plank equation is an extension of Ficks Second law, in the absence of migration but leaving all terms that can be operated on by the gradient or Laplacian we obtain

$$\frac{\partial C_m}{\partial t} = \nabla^2 (D_m C_m) - \vec{V} \nabla (C_m) \tag{9}$$

Equation 9 is solved under the initial condition $C_m(x,y,z,t=0)=C_m^*$ where $C_m^*$ represents the initial concentrations of species $O$ and $R$. The flux balance boundary condition is applied

$$D_O \nabla C_O\Big|_{at\ \ the\ \ electrode} = D_R \nabla C_R\Big|_{at\ \ the\ \ electrode} \tag{11}$$

Clearly, the hydrodynamic problem is coupled with the electrochemical problem via the current expression throughout the entire electrolytic (ionic) conductor.

**S3 Meshing the domain**

The mesh region around the working electrode is the most important region in the entire domain. In order to capture the concentration profile correctly the grid resolution must be precise. A smooth transition of the mesh from the working electrode into the bulk solution is important. If the transition is too steep then the solver diverges, while if it is too slow, the number of cells increases to an unmanageable level. For our purposes we broke the domain up into two smaller regions with different meshing characteristics. The first region was directly around the working electrode, the region discussed is slightly bigger than the working electrode diameter wide and two working electrode diameter long. In this region the first node was placed approximately 5 μm away from the working electrode in the normal direction. From this, a HalfCosinus2 algorithm was employed to vary the spacing of the nodes smoothly away from the working electrode. The HalfCosinus follows a spacing pattern of a half Cosine function in which the user is allowed to vary ratio in which the cosine function is applied. This provided the smoothing in order to grow the cells to a maximum size set by the user such that the fewest number of cells are used. The total number of cell in the mesh was approximately 900,000. At one end the spacing is much larger than that at the other end. At the end of the half cosine region the volume cells were set to a maximum size, meaning that the meshing software would fill in the rest of the domain (automated) but would not allow the size of the elements to be bigger than that specified. The maximum size allowed for this geometry was 0.8; this may seem arbitrary but it is based off experience in how many cells this would create and the size needed to obtain an accurate picture of the physics. Notice though that no units are attached to any of the numbers mentioned, this is because when drawing in ANSYS® ICEM CFD™ there are no units attached to geometry. The geometry and mesh are drawn using whatever means the user requires and then in the finite-volume software a scaling factor is applied in order to size the mesh to the appropriate scale. The ANSYS® ICEM CFD™ then makes up the rest of the domain in order to satisfy the constraints.

By varying the grid size and resolution, it was determined that in order to obtain the correct concentration gradients and currents predicted by theory (e.g., via the Cottrell

equation after a potential step in the absence of convection) at least one node should be placed inside the diffusion layer. By using the random walk equation (eq 7), where $\Delta$ is the diffusion layer thickness, and

$$\Delta = \sqrt{2Dt} \tag{S8}$$

$D$ the diffusion coefficient. It is calculated that for the integration time step used in the simulations ($t$=0.01s) the diffusion layer thickness in the very first step is approximately 7 μm, therefore the first node satisfies the condition above.

# VITA

Cajon Gonzales was born in Lincoln Nebraska, on May 31, 1985. In 2009 he received his Bachelor's of Science in Mechanical Engineering from Missouri University of Science and Technology. In 2010 he began research with Dr. Isaac using CFD to analyze electrochemical cells. He worked for Bettis Atomic Power Laboratory in the summer of 2011. In May 2012 he received his M.S. in Mechanical Engineering degree for Missouri University of Science and Technology.

He has one paper under review in JACS. He will also be married in June 2012 to Anna Lepley. Cajon enjoys, fishing, hunting, racquetball, tennis, and riding his motorcycle. He accepted a position at Bettis Atomic Power Laboratory.